




Cite this: *Nanoscale*, 2024, **16**, 17954

A buffering PVDF-HFP-based gel polymer electrolyte for stable and flexible lithium batteries†

Ahmad Shokrieh,^{‡a,b} Ruichao Lu,^{‡a,b} Binbin Zhang,^a Bharat Prasad Sharma^c and Zhixiang Wei ^{*a,b}

Flexible lithium batteries (FLBs) are highly regarded as potential candidates for next-generation batteries due to their versatility in various applications. However, the main focus in the development of FLBs lies in addressing mechanical challenges such as crack propagation under conditions of flexibility and stretchability. Herein, this work presents a novel design of a gel polymer electrolyte (GPE112) film prepared by solution-casting methods. The GPE112 film shows high ion conductivity of $2.12 \times 10^{-4} \text{ S cm}^{-1}$, a window voltage stability of $\sim 4.6 \text{ V}$, and compatibility with various commercial cathodes such as LiFePO_4 , LiCoO_2 and $\text{LiNi}_{0.8}\text{Co}_{0.1}\text{Mn}_{0.1}\text{O}_2$. On the other hand, the mechanically robust GPE112 film exhibits elongation at break of $\sim 41\%$, making it a potentially superior alternative to a commercial polypropylene (PP) separator. Furthermore, through finite element method (FEM) simulation, the utilization of a hot-pressed polymer electrolyte in conjunction with a cathode active layer demonstrates the potential to mitigate crack propagation and prevent delamination, leading to the development of flexible batteries with robust structures. Generally, the investigation demonstrates that the prepared GPE112 film provides potential application in safe FLBs no matter the electrochemical or mechanical properties.

Received 17th May 2024,
Accepted 24th July 2024

DOI: 10.1039/d4nr02119c

rsc.li/nanoscale

1. Introduction

Flexible lithium batteries (FLBs) are regarded as potential candidates for next-generation batteries due to their versatility in various applications. The adaptability of FLBs allows for their customization in terms of size and shape, providing significant opportunities for diverse industrial applications.¹ However, the primary focus within the realm of FLBs lies in addressing the mechanical challenges. These challenges include ensuring great flexibility and good stretchability,² preventing crack propagation under bending or torsional loads,³ managing thermo-mechanical challenges for safety considerations,^{4,5} achieving light-weight and ultra-thin⁶ properties with optimal encapsulation, *etc.* Researchers and industry professionals need to tackle these mechanical issues in order to fully harness the potential of FLBs in future energy storage solutions.

Numerous significant mechanical challenges have been identified that directly impact the performance of flexible batteries.⁷ Structural challenges involve ensuring the mechanical integrity of each component of the flexible battery, such as avoiding delamination between the active layer and current collector, crack growth in the active layer of electrodes, uncontrollable lithium dendrite growth, unstable interfaces between solid-state electrolytes and electrodes, *etc.* Recently, various approaches and strategies have been reported to overcome these challenges and enhance the stability of all components of FLBs. Excessive mechanical loads may lead to delamination occurring at the interface between the active layer and the current collector. Song *et al.*⁸ showed how calendaring, a process of applying controlled pressure to the active layer on the current collector surface, effectively prevents mechanical damage in FLBs. Particle cracking in the active layer is also considered as one of the important causes of structural deterioration of FLBs. To address this problem, Liu *et al.*⁹ reported a novel composition design to fabricate a mechanically robust Ni-rich cathode material to avoid cracks growing in cathode materials. Moreover, the uncontrollable growth of lithium dendrites and an unstable solid electrolyte interphase (SEI) contribute to poor mechanical strength. Lu *et al.*¹⁰ demonstrated that a mechanically robust porous polymer electrolyte can physically hinder the growth of Li dendrites due to its superior mechanical integrity. Furthermore, an unstable interface between solid-state electrolytes and electrodes is

^aCAS Key Laboratory of Nanosystem and Hierarchical Fabrication, CAS Center for Excellence in Nanoscience, National Center for Nanoscience and Technology, Beijing 100190, P. R. China. E-mail: weizx@nanoctr.cn

^bUniversity of Chinese Academy of Sciences, Beijing 100049, P. R. China

^cBeijing Key Laboratory of Electrochemical Process and Technology of Materials, College of Materials Science and Engineering,

Beijing University of Chemical Technology, Beijing 100029, China

†Electronic supplementary information (ESI) available. See DOI: <https://doi.org/10.1039/d4nr02119c>

‡These authors contributed equally to this work.



another structural challenge of FLBs. This instability hinders the progress of solid-state lithium batteries. To overcome this issue, Li *et al.*¹¹ fabricated a succinonitrile (SN)-based polymer electrolyte with a cross-linked SN polymer skeleton that has great mechanical strength and inhibits the side reaction between the SN and Li anode.

Like other lithium batteries, another concern about FLBs is safety. Due to the flammable nature of liquid electrolytes, researchers are increasingly focusing on solid polymer electrolytes. Notably, novel polymer electrolytes have gained significant attention as a potential solution to address both safety and performance challenges in FLBs. Key challenges in the application of polymer electrolytes include achieving high solubility of lithium salts, maintaining excellent mechanical properties, ensuring superior electrical and thermal stability, and optimizing interfacial compatibility. Two decades of research results show that poly(vinylidene fluoride-co-hexafluoropropylene) (PVDF-HFP) is one of the most promising polymers that has great potential to be selected as a polymer matrix in various polymer electrolyte structures.¹² The PVDF-HFP-based polymer electrolytes offer several advantages, including the ability to prevent dendrite growth,^{10,13} high ionic conductivity, and the suppression of lithium pulverization during cycling due to their composite 3D structure.^{14,15} Due to the high density of polarizable fluorinated groups and high dielectric constant of PVDF-HFP, it is a widely used polymer in lithium metal batteries,¹⁰ *etc.*^{16,17} It is no wonder that one can find the footprint of PVDF-HFP in many applications such as Li–O₂ batteries,¹⁸ sodium batteries,¹⁹ and supercapacitors.²⁰

This study aimed to address two significant mechanical challenges in FLBs, including crack growth and delamination. To mitigate these issues, a gel polymer electrolyte (GPE) film was fabricated using a solution-casting method with mechanically robust PVDF-HFP polymer. The GPE, which exhibits excellent electrochemical performance, was then incorporated into a finite element simulation to investigate its impact on bending stress within the composite layers. Furthermore, the interfacial contact was improved by the hot-pressing method, which could help to enhance the battery's performance and suppress growing cracks in the cathode active layer. Specifically, hot-pressing the GPE with the cathode active layer could make a buffering structure that potentially mitigates crack propagation, inhibits dendrite growth, and prevents the delamination of the cathode active layer when subjected to bending *via* cyclic loading. The outcomes of this study may contribute to the development of flexible batteries from both the electrochemical and mechanical points of view.

2. Experimental section

2.1 Materials

PVDF-HFP (Sigma-Aldrich, average M_w ~400 000, average M_n ~130 000, pellets), bis(trifluoromethanesulfonyl)imide (LiTFSI), *N,N*-dimethylformamide (DMF, Aldrich), Li foil

(China Energy Lithium Co., Ltd), polyvinylidene difluoride (PVDF, Alfa Aesar), carbon black (Super P), LiCoO₂ (LCO), LiFePO₄ (LFP), and LiNi_{0.8}Co_{0.1}Mn_{0.1}O₂ (NCM811) were used for this study. All materials and chemicals were used as received.

2.2 Preparation of the GPE

The preparation was carried out in a glove box under argon flow with 0.1 ppm water and 0.1 ppm oxygen. The GPE was prepared *via* a solution-casting method. First, 1 g of PVDF-HFP was dissolved in 5 mL of DMF, followed by mechanical stirring for 2 hours at 60 °C to obtain a homogeneous solution. Then, different ratios of LiTFSI salt (0.9, 1.2, 1.5, and 1.8 g) were added and the solution was further mixed after stirring for 30 minutes. Subsequently, the prepared homogenized viscous mixture was cast onto a clean glass plate using a doctor blade. Finally, the obtained film was dried for 24 hours in a vacuum oven at 80 °C to remove the residual free solvent. The uniform GPE film (35–40 μm in thickness) was punched into discs with a diameter of 16 mm for further use.

2.3 Materials characterization

The cross-sectional morphology of the GPE was characterized using a field-emission scanning electron microscope (SEM, Hitachi SU8220). Raman spectroscopy was conducted using a Raman shift graph (Spectrum One, PerkinElmer Instruments Co., Ltd). X-ray diffraction (XRD) patterns were acquired on an X-ray diffractometer (Rigaku D/max-2500). The mechanical tests were performed using a universal tensile testing machine (Zwick/Roell Z010, Germany) and dynamic mechanical analysis (DMA) was conducted using a TA Instruments (Q800). Thermal gravimetric analysis (TGA, TA Instruments SDT Q600) was carried out on cured GPE to analyze the weight fraction of DMF inside the GPE. A differential scanning calorimetry device (DSC, TA Instruments Q2000) was used to obtain the crystalline temperature, T_c .

2.4 Electrochemical tests

CR2032-type coin cells were assembled in an argon-filled glove box and used to assess the electrochemical performance of polymer electrolytes. The EIS measurements were conducted on an electrochemical workstation. Battery performance was examined on a LAND2001 battery tester using as-prepared GPE. The LFP, LCO and NCM cathodes were prepared by mixing active materials, Super P and PVDF, in the ratio of 80 : 10 : 10, with *N*-methyl-2-pyrrolidone (NMP) as the solvent. The LFP/Li, LCO/Li, and NCM/Li full batteries were subjected to cycling within the voltage ranges of 2.5 V to 4.0 V, 3 V to 4.2 V, and 3 V to 4.2 V, respectively (Fig. S1†).

3. Results and discussion

3.1 Preparation and characterization of the GPE

In GPEs, the dissolved salt influences the charge transport, viscosity and even the segmental motion of the polymer matrix,



which induces quite different physical and chemical properties. Therefore, various mass ratios of PVDF-HFP matrix to lithium salt were explored as follows: 1 : 0.9, 1 : 1.2, 1 : 1.5, and 1 : 1.8, and denoted as GPE109, GPE112, GPE115, and GPE118, respectively. Fig. 1a illustrates the Nyquist plots of the above samples, and the calculated ionic conductivities based on stainless steel SS/GPE/SS cells using electrochemical impedance spectroscopy (EIS) tests in the frequency range of 100 kHz to 10 MHz with an amplitude of 10 mV at room temperature (RT) and calculated using eqn (1), where σ represents the ionic conductivity, R is the resistance value of the bulk GPE, and L and S are the thickness and effective contact area between the GPE and SS. The inset in Fig. 1a shows a critical tendency when increasing the salt concentration. Among the samples, the intermediate GPE112 exhibited the highest ionic conductivity of $2.21 \times 10^{-4} \text{ S cm}^{-1}$ at RT, which might be the trade-off behavior of the ion transference and the electrolyte viscosity induced by salt content enhancement.

$$\sigma = \frac{L}{S \times R} \quad (1)$$

In addition to the high ionic conductivity, a wide electrochemical window is also desirable for electrolytes. Linear sweep voltammetry (LSV) values were also obtained by scanning assembled SS/GPE/Li asymmetric coin cells at a sweep rate of 0.1 mV s^{-1} in a voltage range of 2 to 6.0 V (vs. Li/Li⁺) at RT. As observed from Fig. 1b, with GPE112, a mild current

peak is observed at 4.6 V (inset in Fig. 1b) without obvious current fluctuation, suggesting that it is electrochemically stable. Otherwise, the interaction between the high-content PVDF-HFP matrix and LiTFSI salt further slows up the decomposition of PVDF-HFP under high voltage. Therefore, the electrochemical stability window of GPE112 is wide enough to meet the requirements of most commercial cathodes (such as LFP, LCO, and NCM). Synthetically, by considering the above electrochemical factors, the GPE112 sample was used in subsequent tests if there was no special mention in this paper to the contrary. Furthermore, to gain a better understanding of Li⁺ transport at the interface of the GPE112 polymer electrolyte, theoretical calculations of the binding energy of lithium ions have been performed, which are presented in Fig. S2.† Also, frontier molecular orbitals (FMOs) and electrostatic potential (ESP) maps are provided in the ESI† to illustrate the distribution of electrons and provide a visual representation of the electron density distribution (Fig. S3 and S4†).

The crystalline phase of GPE112 was characterized by X-ray diffraction (XRD). As shown in Fig. 1c, the XRD pattern shows a typical semi-crystalline state and two crystalline phases of PVDF-HFP. The weak diffraction peak at 18.4° corresponds to the (020) plane of the nonpolar α phase, while the intense peak at 20.0° corresponds to the (110/200) planes of the β phase.^{21,22} Furthermore, Raman spectroscopy was also conducted to confirm the crystalline phase of the GPE. As seen

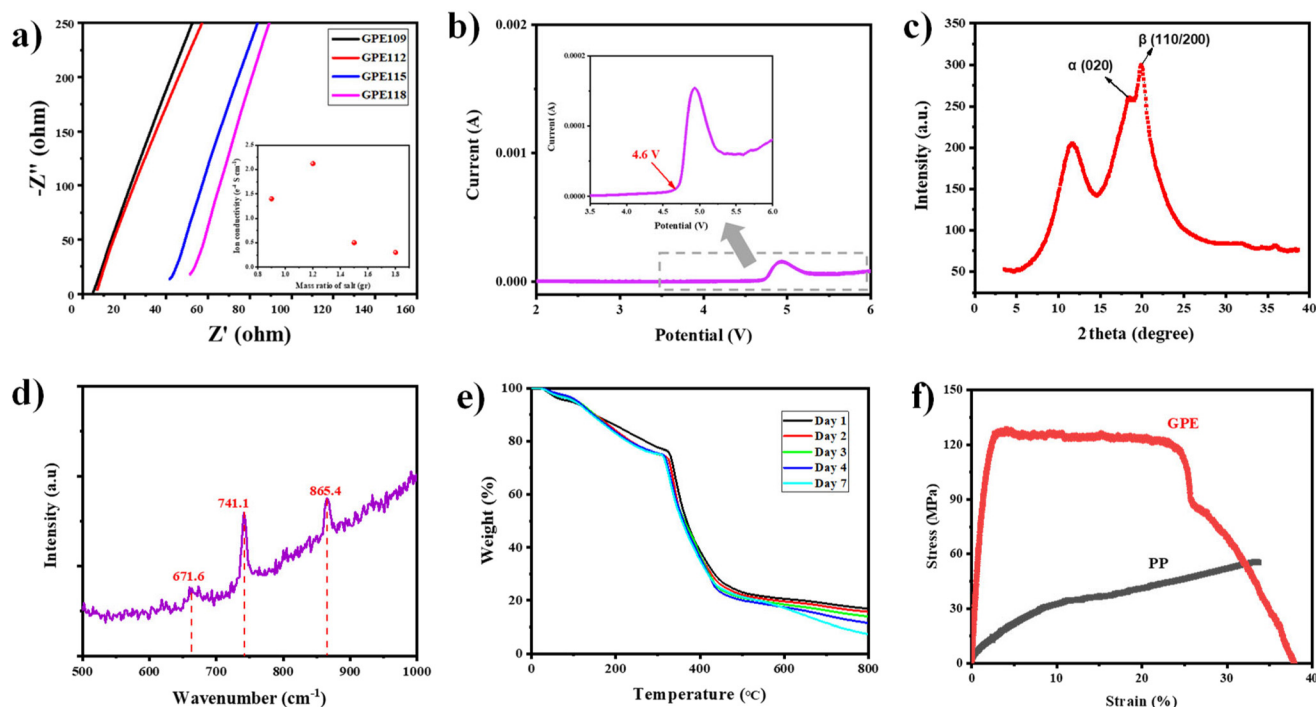


Fig. 1 (a) Electrochemical impedance spectra (EIS) of different ratios of LiTFSI salt in the PVDF-HFP matrix. Inset: ionic conductivity calculated for GPE109, GPE112, GPE115 and GPE118 at RT. (b) Linear sweep voltammetry curve of GPE112 scanned at a sweep rate of 0.1 mV s^{-1} in the range of 2 to 6 V at RT. Inset: zoomed-in profile of the 3.5 to 6 V range with an accurate current range of around 0.0001A. (c) XRD pattern of GPE112. (d) Raman spectroscopy graph of GPE112. (e) TGA results of GPE112 to measure the residual DMF over one week. (f) Stress–strain diagrams of the GPE film and the PP separator.



from Fig. 1d, the Raman peak located at around 865 cm^{-1} confirms the existence of the β phase in the GPE, which is in accordance with the XRD results. Notably, the β phase of PVDF-HFP has strong interactions with Li^+ because of its high polarity, which is beneficial for inducing uniform Li-ion flux²³ and improving the cyclability of the Li anode. The peaks at 671.6 cm^{-1} and 741.1 cm^{-1} can be attributed to $\text{Li}^+\cdots\text{O}=\text{C}-\text{N}$ coordination and the shifted band of $\text{O}=\text{S}=\text{O}$, respectively, due to the solvated complex between LiTFSI and DMF.²⁴ These results can prove that all the DMF might exist as a bound type in the GPE. In the subsequent phase, the weight percentage of DMF solvent in GPE112 was analyzed using TGA. The boiling temperature of DMF is approximately $150\text{ }^\circ\text{C}$, and all GPE samples were cured in a vacuum oven for 24 hours at $80\text{ }^\circ\text{C}$. In order to determine the remaining amount of DMF solvent within the gel polymer electrolyte, the test setup involved raising the temperature to $350\text{ }^\circ\text{C}$ and allowing it to stabilize for 10 minutes before further increasing the temperature to $800\text{ }^\circ\text{C}$ at a heating rate of $10\text{ }^\circ\text{C min}^{-1}$ under a nitrogen atmosphere. To provide a more accurate estimation of DMF present in the gel polymer electrolytes, the weight percentage lost between $80\text{ }^\circ\text{C}$ and $350\text{ }^\circ\text{C}$ was measured to obtain a reliable assessment of the weight percentage of DMF within the gel polymer electrolyte. Each sample was subjected to five tests each day, enabling the determination of an average value for the weight percentage of DMF solvent present in the GPE112 samples. The weight percentage and mass of DMF solvent can be calculated from the TGA thermogram (Fig. 1e) using the following equation:

$$M_{\text{DMF}} = M_{\text{GPE112}} \times (R_{80^\circ\text{C}} - R_{350^\circ\text{C}}) \quad (2)$$

where R represents the residue percentage. In order to make sure of the residual DMF content and its variation in the GPE, the percentage of DMF was detected specifically and observed to be maintained at about 20 wt% for one week (Table S1†). Such a small quantity of DMF solvent could reduce the flammable hazard of the electrolytes. Moreover, the presence of DMF also facilitates the GPE membrane having a smooth surface and effectively reduces the shear forces with a cathode and anode during bending load. Based on the mass content of DMF, the molar ratio of DMF and LiTFSI is calculated to be about 2 : 1, indicating almost no free DMF in the prepared GPE112.²⁵ These results are in accordance with the Raman results.

Due to the electronic insulating function between the cathode and the anode, the GPE should be able to withstand various mechanical deformations and keep its structural integrity in potential flexible applications. Compared with other polymer matrices, PVDF-HFP presents superior mechanical properties with no need for incorporation of any extra additives. As seen from the stress–strain profiles shown in Fig. 1f, the GPE has better mechanical properties than those of the PP separator in terms of Young's modulus, strength, and elongation at break. Table S2† lists the specific data calculated from the stress–strain profiles. In the present scenario, it is feasible

to incorporate this resilient GPE to alleviate the stress of other contact layers when subjected to bending loads. As a result, cracking of current collectors and even the delamination of active layers can be effectively mitigated to avoid structural destruction and internal short circuits in subsequent deformation applications. Undoubtedly, the forthcoming generation of lithium-ion batteries necessitates attaining ultra-thin, ultra-light, and complete flexibility features as crucial objectives. Consequently, the implementation of a GPE as an active layer holder, characterized by its exceptional mechanical properties, emerges as a promising process worthy of further exploration in future research.

3.2 Optimization of battery performance by hot pressing process

One of the most critical points for flexible batteries is the delamination phenomenon of the active layer in different bending states. Researchers have explored different materials to try to prevent this phenomenon.^{26,27} The active layer is very brittle because it is made of functional powders glued by little inactive polymer binder (around 5% to 10% of the whole active layer mass). On the other hand, poor adhesion between the current collectors and the active materials is caused due to their smooth surfaces. One of the most effective strategies to solve the delamination problem is to optimize the connection of the different layers.^{28,29} Herein, hot pressing was employed to achieve close contact between the layers, improving adhesion and overall stability. Therefore, a trial-and-error method was used to uncover the best practices for the hot-pressing process. Some parameters are crucial for this method: pressure, the thickness of the composite layer, and temperature at the press. To prepare the sample with the desired quality, three pressures of 0.5, 1, and 2 bar were considered. Also, the applied temperatures during the hot press were 100, 150 and $180\text{ }^\circ\text{C}$, respectively. Finally, the whole process was optimized by testing and characterization of the samples (Table S3†). In this case, the melting temperature (T_m) and crystalline temperature (T_c) were first measured with a DSC device (TA Instruments Q2000, USA) in temperature modulation mode under a nitrogen atmosphere (60 mL min^{-1}). Approximately 5 to 10 mg of the samples were sealed in aluminum pans. Modulated DSC measurements were carried out in the temperature range of 0 to $200\text{ }^\circ\text{C}$ at a heating rate of 10 K min^{-1} with an amplitude of 0.5 K and a period of 60 s. According to Fig. S5,† the DSC thermogram of GPE112 exhibits two distinct peaks: an endothermic peak at approximately $78.8\text{ }^\circ\text{C}$, corresponding to the crystalline transition temperature, and an exothermic peak at approximately $109\text{ }^\circ\text{C}$, indicating the melting temperature.³⁰ In the next step, by hot-pressing the cathode active layer to the GPE112 film, the active layer and polymer electrolyte can be well combined and formed into a uniform thin layer, which will help to prevent the rapid growth of cracks in the active layer.

The resulting samples were named cathode active layer–GPE, and cathode active layer–PP and abbreviated as CAL–GPE and CAL–PP, respectively. Optical photographs reveal that the



CAL was well pressed onto the GPE surface. This is evidenced by the strong adhesion between the PVDF binder (inside the active layer) and the PVDF-HFP (acting as the GPE matrix). In order to validate this observation, a fatigue test was conducted on both the CAL–GPE and CAL–PP samples involving 10 000 cycles of bending. Subsequently, the samples were frozen in liquid nitrogen and divided into two parts to expose their cross-sections for SEM analysis. Fig. 2a demonstrates that the CAL–GPE sample displays uniform and well-connected surfaces between the CAL and GPE, thereby preventing the separation or non-uniformity of the active layer during multiple bending stress. However, Fig. 2b clearly depicts the emergence of growing cracks between the surfaces of the CAL–PP sample. This evidence reveals that GPE112 can effectively protect the active layer and inhibit crack propagation under bending loads, owing to the optimal bonding between PVDF and PVDF-HFP.

The active layer was subjected to hot pressing onto a commercial separator made of polypropylene (PP) and a gel polymer electrolyte (GPE112) at a temperature of 150 °C under a pressure of 0.5 bar, respectively. Then, the aluminum substrate was peeled from both samples (Fig. 3a). In order to evaluate the electrochemical performance of the CAL–GPE sample, two test concepts were devised in the subsequent step. The CAL–GPE film demonstrated excellent stackable features, which lead to a higher output voltage and thus a higher energy. To visually manifest this unique advantage, first, mono-cell and bipolar-cell full batteries were assembled (Fig. 3b) using thinner structures. As shown in Fig. 3c and d, the voltage values of open circuits (VOCs) of mono-cells and bipolar-cells were found to be 3.05 and 5.87 V, respectively. Second, three commercially available active layers (LFP, LCO,

and NCM) were hot-pressed onto GPE112 films, and their coin cells were assembled with lithium foil as the anode. These samples were denoted as LFP–GPE112/Li, LCO–GPE112/Li, and NCM–GPE112/Li, respectively. Their rate performance, as shown in Fig. 3e, indicates that the rate test conducted on these three samples demonstrated acceptable discharge capacity.

3.3 The stability of the lithium anode and applications in coin cells

The interfacial problem is significant for the GPE due to the solid–solid contact between layers, which will influence electrochemical kinetics and the stability of the batteries. The stability of GPE112 towards the Li anodes was investigated by assembling Li/GPE112/Li symmetrical batteries, and the galvanostatic cycling was further carried out with a capacity of 0.1 mA h cm^{−2} at a current density of 0.1 mA cm^{−2}. An Li/Li symmetric cell shows a stable voltage profile for 1300 h (650 cycles) (Fig. 4a), and the initial overpotential is only about 100 mV. The stable performance of GPE112 indicates its compatibility towards lithium metal.

To demonstrate the potential application of the GPE in FLBs, LFP/GPE112/Li, LCO/GPE112/Li, and NCM811/GPE112/Li coin-cell batteries were assembled and their electrochemical performances were investigated. The voltage range and cyclability performance of the above batteries are summarized in Table S4.† As shown in Fig. 4b, LCO/GPE112/Li exhibited excellent rate performance compared to LFP/GPE112/Li and NCM/GPE112/Li. It is observed that GPE112 exhibits good compatibility with NCM and LCO batteries, demonstrating its potential applications at high voltages. Their stability performance was evaluated at 0.2 C and 0.5 C for 100 cycles. As shown

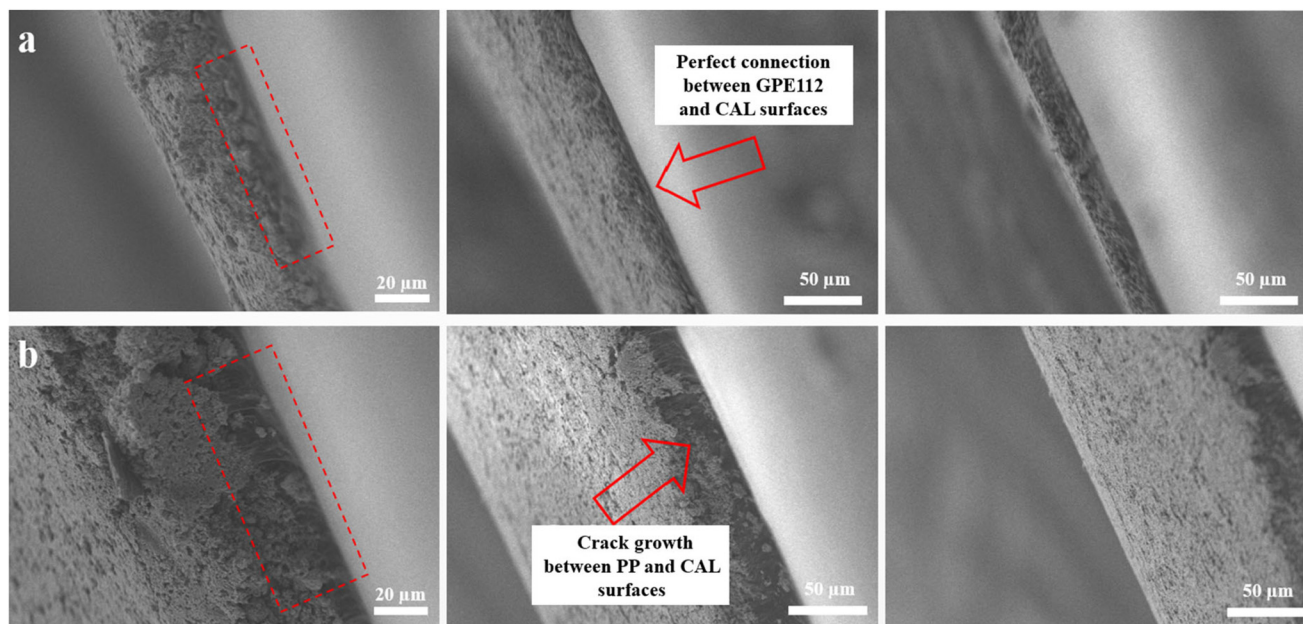


Fig. 2 SEM cross-sectional images of (a) the CAL–GPE112 sample (the perfect connection between GPE112 and CAL surfaces), and (b) the CAL–PP sample (showing crack growth between the PP and CAL surfaces).



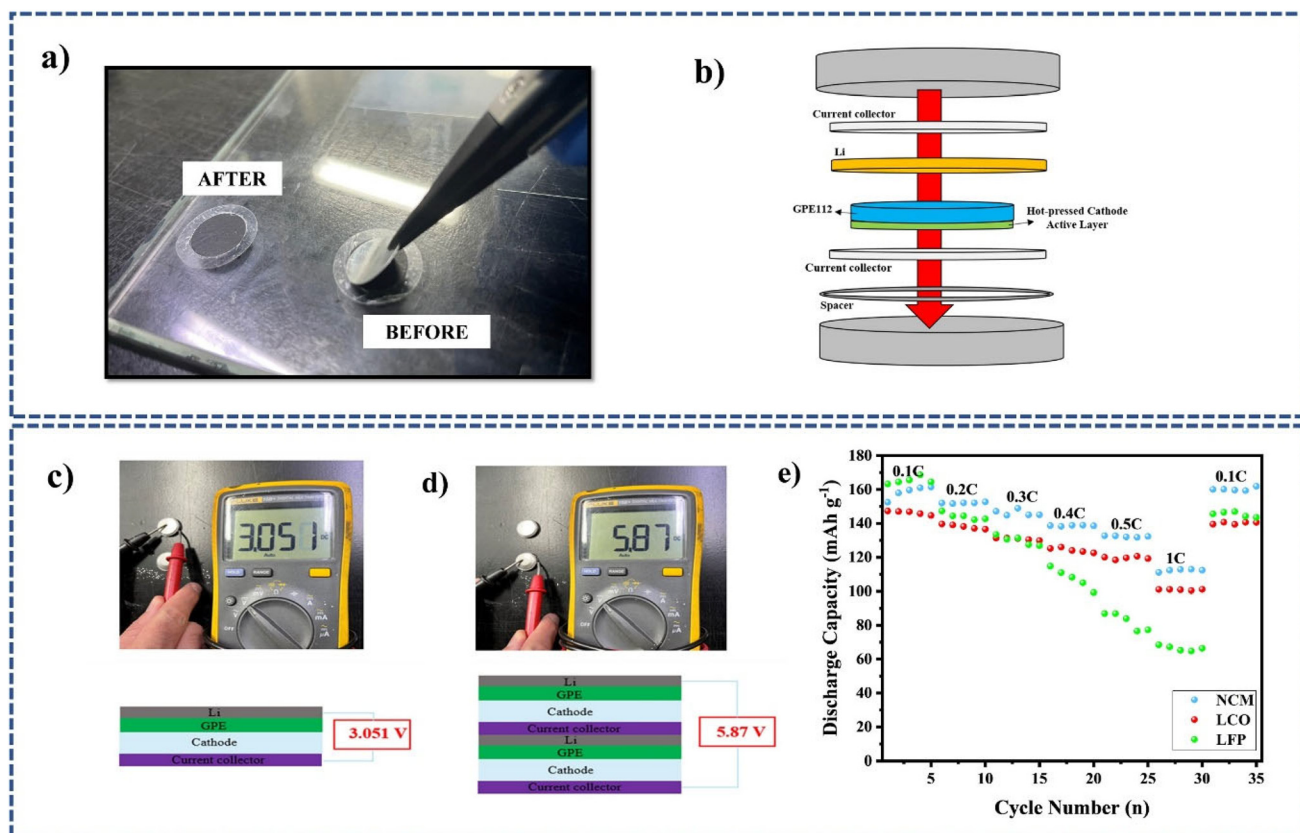


Fig. 3 (a) Hot-pressing the active layer on GPE112 film and peeling off the aluminum metal substrate. (b) Sketch of the assembled CAL-GPE112 full cell. (c) Mono-polar and (d) bipolar CAL-GPE112/Li full cell structures and their VOC values. (e) Rate tests of hot-pressed CAL-GPE112/Li coin cells.

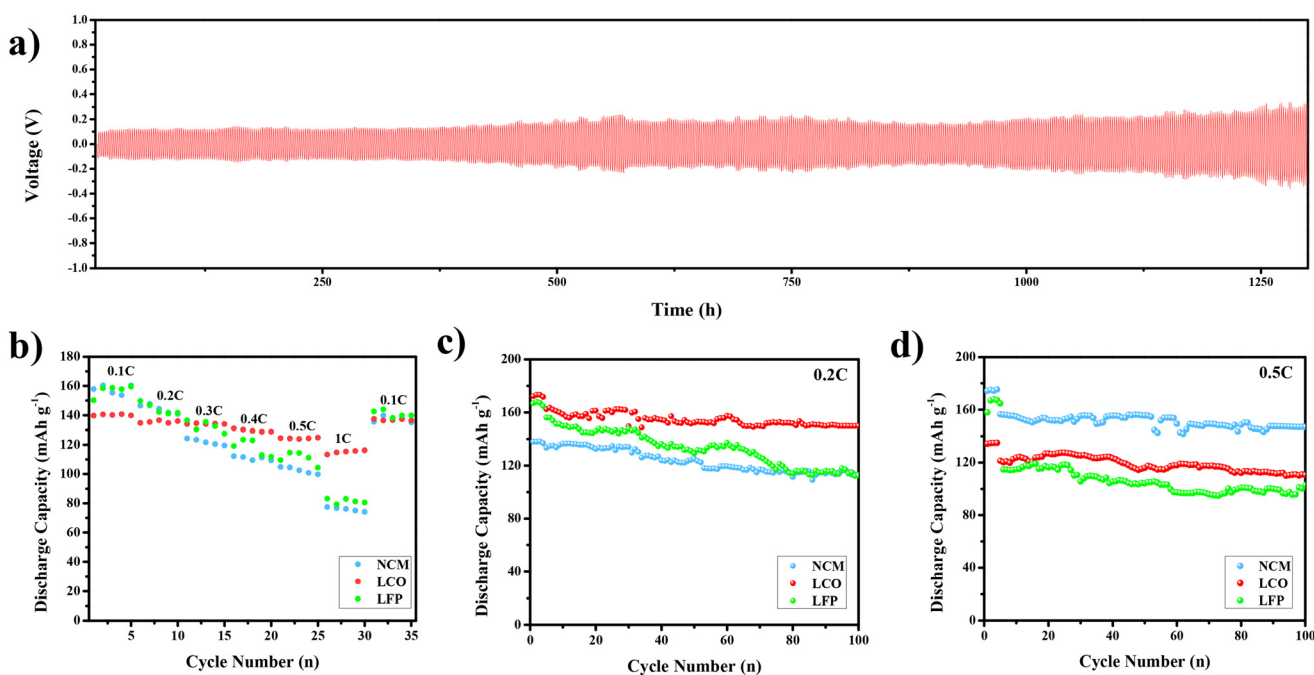


Fig. 4 GPE112 results: (a) galvanostatic cycling performances of Li/Li symmetric cells; (b) rate performances; stability tests of 100 cycles at (c) 0.2 C and (d) 0.5 C with different commercial cathodes (LFP, LCO and NCM).



in Fig. 4c and d, the NCM/GPE112/Li cell displays the greater stability. Comparatively, the LCO/GPE112/Li cell demonstrates favorable performance when evaluating results of both the rate and stability tests.

3.4 Flexible batteries

In the following step, pouch cells were assembled with LFP and LCO as cathode layers and lithium foil as the anode. GPE112

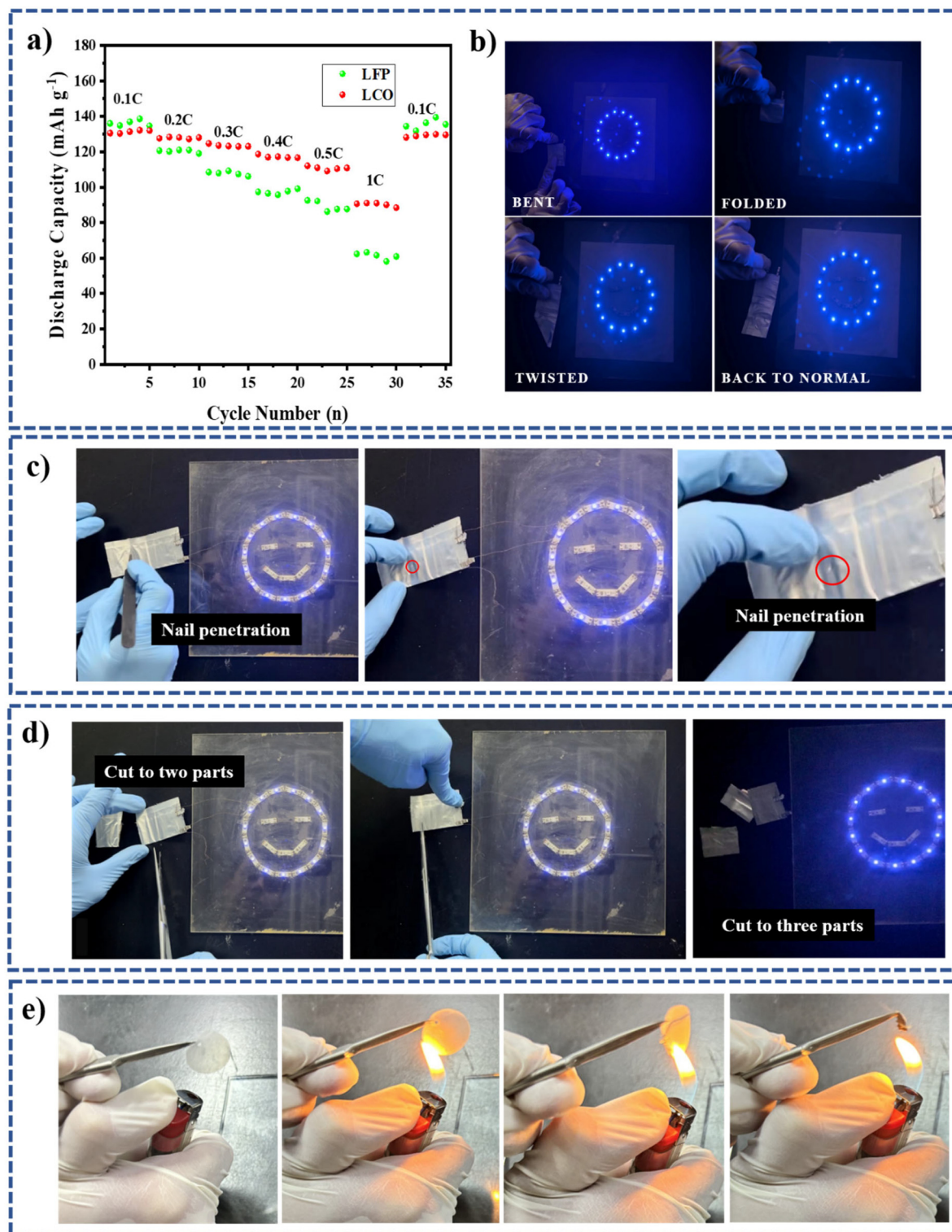


Fig. 5 (a) Rate tests of LFP/GPE112/Li and LCO/GPE112/Li pouch cells; (b) photographs showing the great performances of a pouch cell in bent, twisted, folded, and back to normal shape configurations; (c) nail penetration test; (d) cutting test on the pouch cell; and (e) burning test on the GPE112 film.



was rolled around the cathode and hot-pressed at 150 °C under 0.5 bar pressure to enhance the adhesion force. Fig. 5a presents the rate capacity of the pouch cells with the LFP and LCO cathodes. These data offer insights into the performance of the flexible battery. Furthermore, the flexibility of the pouch cell was assessed by subjecting it to bending, folding, twisting, and returning it to its original shape, as depicted in Fig. 5b. It remained functional in all circumstances, and there were no failures. Lastly, in order to evaluate the safety of the pouch cell, it was subjected to a nail penetration test (Fig. 5c). Then it was cut using scissors, revealing that no combustion occurred due to the absence of liquid electrolyte within the battery (Fig. 5d). In addition, one of the most critical parameters for ensuring safety in flexible battery systems is preventing high-temperature events and combustion accidents. Therefore, the polymer electrolyte must possess inherent safety characteristics, minimizing the risk of high flammability to reduce potential hazards during application. As previously mentioned, the GPE112 film exhibits low content of DMF solvent (approximately 20 wt%) within its gel structure, as determined by TGA. To assess its direct combustion behaviour, a burn test was conducted on the GPE112 sample. As shown in Fig. 5e, the burning process initiates wrinkling of the polymer but the test proceeds smoothly without significant flammability (as demonstrated in Video S1†). This observation indicates that GPE112 exhibits a desirable safety profile, minimizing the risk of uncontrolled combustion and enhancing overall system safety.

Consequently, it can be concluded that the designed pouch cell is completely secure and does not pose any danger to users in the event of its rupture or the development of a hole.

4. Finite element modeling and simulation

As described above, the buffer polymer electrolyte can potentially help to decrease the stress between layers and prevent cracks under bending deformation. To exactly evaluate the effect of the GPE in flexible batteries, experimental and simulation studies were conducted.³¹ Commonly, six loading conditions for pouch cells have been reported in prior literature and these are shown in Fig. S6.† As shown in Fig. S7,† the mechanical properties of each component were first measured using tensile and DMA tests, and the detailed data are presented in Table S5.† Next, the pouch cell was modeled using the finite element method (FEM). The quadratic quadrilateral elements of type S8R were used to mesh the developed model. As shown in Fig. 6a, the three-point bending test of the pouch cell battery was simulated, where the exerted load was applied to the middle part of the battery. The effective length and width of the modeled battery were 80 mm and 20 mm, respectively. The material and thickness of the different layers of the pouch cell are presented in Table S6.†

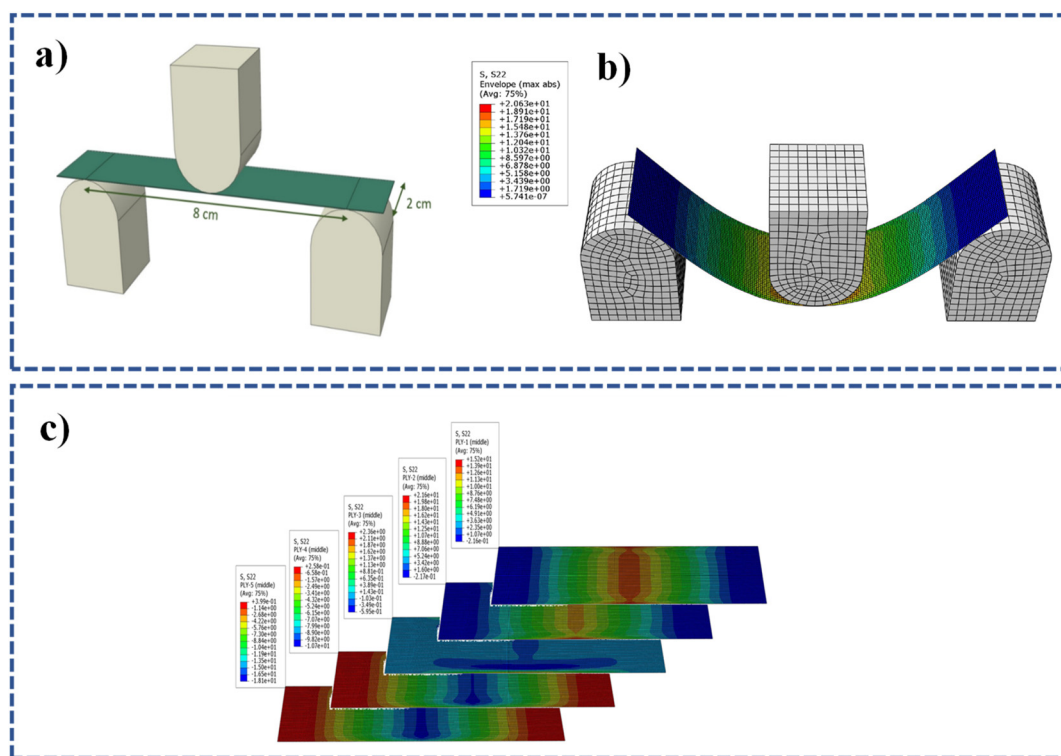


Fig. 6 (a) The finite element model of the simulated three-point bending test of the composite battery, (b) contour plot of bending stress for the battery plate with a 0.020 mm GPE112 layer thickness, and (c) contour plot of bending stress of each layer (composite shell includes: pouch, copper foil, GPE112, aluminum foil and pouch, respectively; Fig. S8–S10†).



Table 1 The induced bending force in different layers by different thicknesses of GPE112 film

Layer number	Components	Bending stress (MPa) (thickness: 0.020 mm)	Bending stress (MPa) (thickness: 0.050 mm)	Bending stress (MPa) (thickness: 0.100 mm)
Layer 1	Pouch	+13.61	+5.29	+2.88
Layer 2	Copper foil	+17.08	+8.15	+5.07
Layer 3	GPE112	-0.10	-0.19	-0.21
Layer 4	Aluminum foil	-9.74	-4.61	-2.67
Layer 5	Pouch	-16.72	-6.40	-3.22

Using models of GPE112 with different thicknesses, their FEM simulations in the three-point bending test of the pouch cell battery (Fig. 6b) were conducted under a constant bending load. The induced bending stress in various layers of the battery by thickness variation is presented in Table 1. The positive signs in Table 1 indicate tensile stress, while the negative signs indicate compressive stress. The incorporation of a polymer electrolyte as an intermediary layer facilitates smoother bending behavior in both the anode and the cathode under applied bending stress. Simulation results, using a GPE112 electrolyte with thicknesses of 20, 50, and 100 μm , reveal a reduction in peak tensile stress within the critical path of the Cu anode layer. These stresses are 17.08 MPa, 8.15 MPa, and 5.07 MPa for the respective thicknesses.

Concurrently, the Al cathode experiences a decrease in compressive stress along its critical path, measuring -9.74 MPa, -4.61 MPa, and -2.67 MPa (Fig. S8-S10[†]). By increasing the thickness from 0.020 mm to 0.050 mm and 0.100 mm, the bending stress was decreased by 53% and 73% in the aluminum layer, and 52% and 70% in the copper layer. The contour plot of the battery plate with a 0.020 mm thickness of GPE112 is shown in Fig. 6c. Analysis of these findings indicates that the anode component is subjected to higher bending stress compared to the cathode. Therefore, it can be concluded that in flexible batteries under bending conditions, anode failure is more probable than cathode failure. It is important to acknowledge that the simulation employed several simplifying assumptions. Notably, while the model incorporates four different components (anode, cathode, polymer electrolyte, and pouch), each with its own coefficient of friction, it does not fully capture the complexities of interfacial interactions. In reality, interlayer friction can significantly influence shear forces within the battery structure, potentially increasing the risk of mechanical failure in the anode or cathode. However, the inherent lubricating properties of GPE112, stemming from its gel-like consistency, suggest minimal interlayer friction, potentially approaching zero. This assumption allows us to minimize the influence of shear stress relative to bending stress within the model. Therefore, while acknowledging the potential role of shear stress, our analysis primarily focuses on the impact of bending stress as the dominant mechanical factor influencing failure in this scenario.

5. Conclusion

In summary, this work presents a GPE112 film based on PVDF-HFP with good electrochemical and mechanical properties, which can potentially solve the challenges faced in FLBs. In terms of electrochemical properties, the prepared GPE112 film exhibits high ion conductivity of approximately $2.12 \times 10^{-4} \text{ S cm}^{-1}$ and exceptional oxidation stability of $\sim 4.6 \text{ V}$, demonstrating its potential compatibility with various commercial cathodes, such as LFP, LCO, and NCM, which are significantly favorable for improving the energy density of FLBs. In terms of mechanical properties, the robust GPE112 film also exhibits high elongation at break of $\sim 41\%$, which is beneficial for preventing active layer cracking under mechanical loading; also bending stress between the layers of pouch cell batteries is alleviated by using the hot-pressing method. Moreover, these characteristics offer advantages in terms of safety and permissibility, even when subjected to nail-punch and cut tests. These superior electrochemical and mechanical properties ensure FLBs have a sustained power supply even in deformation applications.

Author contributions

Z.W. outlined the research idea and supervised the research. A.S. designed and conducted most of the experiments with help from R.L. Z.B.B contributed to the experimental design and helped in the laboratory. B.P.S. performed DFT simulations and analysis. The final version of the manuscript was revised by all authors.

Data availability

The datasets generated and/or analyzed during the current study are available from the corresponding author upon reasonable request. The data supporting the findings of this study, including the electrochemical results, mechanical results, simulation results and SEM images, can be found in the manuscript and the ESI.[†]

Conflicts of interest

There are no conflicts to declare.

Acknowledgements

The authors acknowledge financial support from the National Natural Science Foundation of China (Grant No. 22135001) and the International Partnership Program of the Chinese Academy of Sciences (Grant No. 121D11KYSB20190080).



References

- 1 K. Itani and A. Alexandre De Bernardinis, Review on New-Generation Batteries Technologies: Trends and Future Directions, *Energies*, 2023, **16**, 7530.
- 2 G. Qian, X. Liao, *et al.*, Designing Flexible Lithium-Ion Batteries by Structural Engineering, *ACS Energy Lett.*, 2019, **4**, 690–701.
- 3 F. Pistorio, D. Clerici, *et al.*, Review on the numerical modeling of fracture in active materials for lithium ion batteries, *J. Power Sources*, 2023, **566**, 232875.
- 4 Y. Q. Chen, Y. Q. Kang, Y. Zhao, *et al.*, A review of lithium-ion battery safety concerns: The issues, strategies, and testing standards, *J. Energy Chem.*, 2021, **59**(1), 83–99.
- 5 L. Wen, J. Liang, J. Chen, Z. Y. Chu, *et al.*, Smart Materials and Design toward Safe and Durable Lithium Ion Batteries, *Small Methods*, 2019, **3**(11), 1900323.
- 6 Z. H. Wang, L. Shen, S. H. Deng, P. Cui, *et al.*, 10 μm -Thick High-Strength Solid Polymer Electrolytes with Excellent Interface Compatibility for Flexible All-Solid-State Lithium-Metal Batteries, *Adv. Mater.*, 2021, **33**, 2100353.
- 7 A. Shokrieh, A. Mirzaei, L. Mao, *et al.*, A review of the mechanical integrity and electrochemical performance of flexible lithium-ion batteries, *J. Nano Res.*, 2023, **16**, 12962–12982.
- 8 Y. J. Song, K. Gao, C. W. He, *et al.*, Exploring particle-current collector contact damage in Li-ion battery using DEM-FEM scheme, *Appl. Energy*, 2023, **351**, 121904.
- 9 T. Liu, L. Yu, J. Lu, *et al.*, Rational design of mechanically robust Ni-rich cathode materials via concentration gradient strategy, *Nat. Commun.*, 2021, **12**, 6024.
- 10 R. Lu, A. Shokrieh, C. Li, *et al.*, PVDF-HFP layer with high porosity and polarity for high-performance lithium metal anodes in both ether and carbonate electrolytes, *Nano Energy*, 2022, **95**(1), 107009.
- 11 Z. C. Li, Q. Liu, Y. R. Deng, *et al.*, In situ cross-linked plastic crystal electrolytes toward superior lithium metal batteries, *Mater. Today Energy*, 2023, **31**, 101198.
- 12 W. Liu, C. J. Yi, L. P. Li, *et al.*, Designing Polymer-in-Salt Electrolyte and Fully Infiltrated 3D Electrode for Integrated Solid-State Lithium Batteries, *Angew. Chem., Int. Ed.*, 2021, **60**, 12931–12940.
- 13 Z. C. Li, W. H. Tang, Y. R. Deng, *et al.*, Enabling highly stable lithium metal batteries by using dual-function additive catalyzed in-built quasi-solid-state polymer electrolytes, *J. Mater. Chem. A*, 2022, **10**, 23047.
- 14 Z. Q. Liu, D. C. Guo, W. T. Fan, *et al.*, Expansion-Tolerant Lithium Anode with Built-In LiF-Rich Interface for Stable 400 Wh kg^{-1} Lithium Metal Pouch Cells, *ACS Mater. Lett.*, 2022, **4**, 1516–1522.
- 15 Z. Q. Liu, X. Fu, Z. D. Li, *et al.*, Integrated anode with 3D electron/ion conductive network for stable lithium metal batteries, *Energy Storage Mater.*, 2024, **66**, 103201.
- 16 J. Zhang, Y. Zeng, *et al.*, Polymer-in-salt electrolyte enables ultrahigh ionic conductivity for advanced solid-state lithium metal batteries, *Energy Storage Mater.*, 2023, **54**, 440–459.
- 17 X. Lu, Y. Wang, *et al.*, Polymer-Based Solid-State Electrolytes for High-Energy-Density Lithium-Ion Batteries – Review, *Adv. Energy Mater.*, 2023, **13**, 2301746.
- 18 T. Liu, Z. Chang, Y. Yin, K. Chen, *et al.*, The PVDF-HFP gel polymer electrolyte for Li-O₂ battery, *Solid State Ionics*, 2018, **318**, 88–94.
- 19 J. Kim, Y. Choi, K. Y. Chung, *et al.*, A Structurable Gel-Polymer Electrolyte for Sodium Ion Batteries, *Adv. Funct. Mater.*, 2017, **27**(34), 1701768.
- 20 X. Yang, F. Zhang, L. Zhang, *et al.*, A High-Performance Graphene Oxide-Doped Ion Gel as Gel Polymer Electrolyte for All-Solid-State Supercapacitor Applications, *Adv. Funct. Mater.*, 2013, **23**, 3353–3360.
- 21 S. Dash, H. S. Mohanty, Ravikant, A. Kumar, R. Thmoas, D. K. Pradhan, *et al.*, Ferroelectric ceramic dispersion to enhance the β phase of polymer for improving dielectric and ferroelectric properties of the composites, *Polym. Bull.*, 2020, **78**, 5317–5336.
- 22 S. Badatya, A. Kumar, C. Sharma, *et al.*, Transparent flexible graphene quantum dot-(PVDF-HFP) piezoelectric nanogenerator, *Mater. Lett.*, 2021, **290**, 129493.
- 23 J. Luo, C. C. Fang and N. L. Wu, High Polarity Poly(vinylidene difluoride) Thin Coating for Dendrite-Free and High-Performance Lithium Metal Anodes, *Adv. Energy Mater.*, 2018, **8**, 1701482.
- 24 F. L. Xu, S. G. Deng, Q. Y. Guo, *et al.*, Quasi-Ionic Liquid Enabling Single-Phase Poly (vinylidene fluoride)-Based Polymer Electrolytes for Solid-State LiNi_{0.6}Co_{0.2}Mn_{0.2}O₂||Li Batteries with Rigid-Flexible Coupling Interphase, *Small Methods*, 2021, **5**, 2100262.
- 25 F. Xu, S. Deng, *et al.*, Quasi-Ionic Liquid Enabling Single-Phase Poly(vinylidene fluoride)-Based Polymer Electrolytes for Solid-State LiNi_{0.6}Co_{0.2}Mn_{0.2}O₂||Li Batteries with Rigid-Flexible Coupling Interphase, *Small Methods*, 2021, **5**, 2100262.
- 26 Q. Meng, H. Wu, L. Mao, *et al.*, Combining Electrode Flexibility and Wave-Like Device Architecture for Highly Flexible Li-Ion Batteries, *Adv. Mater.*, 2017, **2**(7), 1700032.
- 27 A. M. Gaikwad, B. V. Khau, G. Davies, *et al.*, A high areal capacity flexible lithium-ion battery with a strain-compliant design, *Adv. Energy Mater.*, 2015, **5**(3), 1401389.
- 28 Q. Meyer, N. Mansor, F. Iacoviello, *et al.*, Investigation of Hot Pressed Polymer Electrolyte Fuel Cell Assemblies via X-ray Computed Tomography, *Electrochim. Acta*, 2017, **242**, 125–136.
- 29 L. Sahu, A. Bhatt, A. Chandra, *et al.*, Hot-pressed sodium ion conducting solid polymer electrolytes: Preparation and materials characterization, *Mater. Today: Proc.*, DOI: [10.1016/j.matpr.2023.05.204](https://doi.org/10.1016/j.matpr.2023.05.204).
- 30 S. Abbrent, J. Plestil, D. Hlavata, *et al.*, Crystallinity and morphology of PVdF-HFP-based gel electrolytes, *Polymer*, 2001, **42**, 1407–1416.
- 31 M. Y. Ali, W. J. Lai and J. Pan, Computational models for simulation of a lithium-ion battery module specimen under punch indentation, *J. Power Sources*, 2015, **273**, 448–459.

